JOURNAL OF GEOPHYSICAL RESEARCH, VOL. 92, NO. B10, PAGES 10,299–10,312, SEPTEMBER 10, 1987

A Numerical Model for Simulating Deformation of Mount St. Helens Volcano

A. PAUL AND J. P. GRATIER

Institut de Recherches Interdisciplinaires de Géologie et de Mécanique
University of Grenoble, France

J. BOUDON

Coyne et Bellier, Paris, France

Previous work on surface deformation associated with volcanic activity has revealed significant departures from ideal elastic and homogeneous behavior. To account for the highly heterogeneous and discontinuous mechanical behavior of volcanic edifices, a numerical model named Bloc was used to model surface deformation data. The basic assumption of this model is that the volcanic edifice behaves mechanically as an assemblage of rock blocks that can move in relation to one another. The well-documented eruption of Mount St. Helens in 1980 was used to test this model and to compare the fit between the observed and computed surface deformation. From the north-south cross section of the volcano, several two-dimensional models were developed to study the effect of various parameters (geometry, boundary conditions, coefficient of friction, etc.). The models were loaded with a step-by-step increasing internal pressure simulating the intrusion of magma within the volcano and with a horizontal acceleration simulating an earthquake. The deformation and failure patterns are highly dependent on the coefficient of friction on block boundaries. For the lower value of this coefficient (0.5), a good fit is found between the observed and computed surface displacements. The failure mode by gravitational sliding of the north flank is obtained with internal pressure loading alone as well as with internal pressure and an earthquake trigger. However, the second kind of loading gives a better fit with the particular deformation pattern observed.

INTRODUCTION

Measurement of surface deformation linked to volcanic activity is one of the most widely used techniques for estimating eruption hazards and understanding volcanic processes. Since these deformations usually arise from movements of magma within the volcanic edifice, their study can yield important results concerning the internal structure of the volcano. Much work has already been done to provide a clearer picture of the relationship between measured surface displacements and the position or geometry of the sources of deformation. Several mechanical models of the structure of volcanoes have been developed, making it possible to calculate the theoretical displacement field induced on the surface by intrusions of various shapes. *Mogi* [1958] was the first to compute surface displacements associated with a point source of inflation embedded in an elastic half space. *Dieterich and Decker* [1975] were the first to use the finite element method to simulate the displacement field produced by intrusions of various geometries on the free surface of a semi-infinite elastic half space. More recently, *Pollard et al.* [1983] have calculated the stress field in addition to the displacements resulting from a dike intrusion in an elastic half space. Finally, a three-dimensional model of surface subsidence generated by the withdrawal of magma from a sill-like storage compartment has been developed by *Ryan et al.* [1983]. These models are commonly used to deduce geometric characteristics of the intrusion giving the best fit between the computed and measured surface displacement fields. *Fiske and Kinoshita* [1969], for example, used Mogi's model to locate a point of inflation within Kilauea volcano (Hawaii), whereas *Murray and Pullen* [1987] have applied Dieterich and Decker's calculations to determine the three-dimensional shape and position of the feeder conduit of Mount Etna's 1983 eruption. A more sophisticated way of locating the centers of intrusive activity by a least squares inversion technique was applied to Kilauea by *Dvorak et al.* [1983].

Although this paper deals with the mechanical modeling of surface deformations associated with volcanism, our approach is quite different from the previous ones. Two points of comparison may be noted.

1. In contrast to the above models, we include the topography of the volcano in the deformation model. Because gravitational loads are incorporated in the stress balance, perturbations of the stress field resulting from these topographic features have been accounted for.

2. We regard the volcanic edifice as a heterogeneous and fractured medium because it is composed of superimposed lava flows cut through by dykes and sill swarms, fractured by repeated intrusions of magma. These numerous discontinuities play an important part in the deformation pattern but were totally neglected in previous models. Moreover, *Pollard et al.* [1983] pointed out discrepancies between the theoretical displacements computed by continuous models and the observed natural deformations. These authors showed that a good fit cannot be found between natural and theoretical vertical displacement profiles when they cross open cracks or normal faults. This simply shows that when the medium is assumed to be continuous, the model cannot predict discontinuous surface displacement fields that, however, characterize the mechanical behavior of volcanoes. A more realistic model thus has to deal with a disjointed and heterogeneous medium.

Such a mechanical model, named Bloc, was developed for applications in civil engineering in 1979 by Coyne et Bellier, Consulting Engineers, Paris [*Pouyet et al.*, 1983]. Its basic principles and the procedure used by the computer program

Paper number 5B5867.
0148-0227/87/005B-5867$05.00

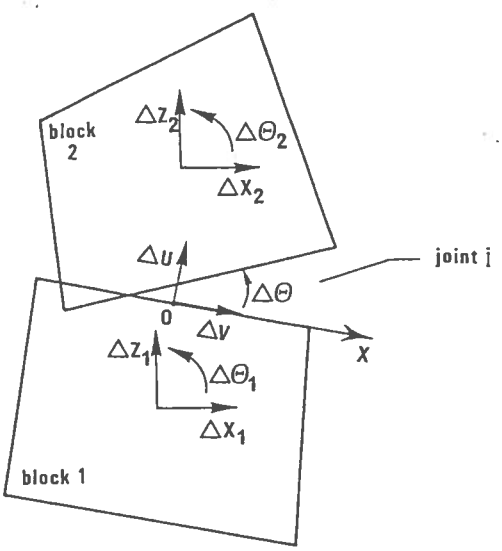

Fig. 1. Definition of the parameters characteristic of the state of deformation of a joint. Here ΔX_1, ΔZ_1, $\Delta\theta_1$, ΔX_2, ΔZ_2, and $\Delta\theta_2$ are displacements and rotations of the two blocks. The ΔU, ΔV, and $\Delta\theta$ are relative displacements and rotation of the two faces of the joint measured at its midpoint 0.

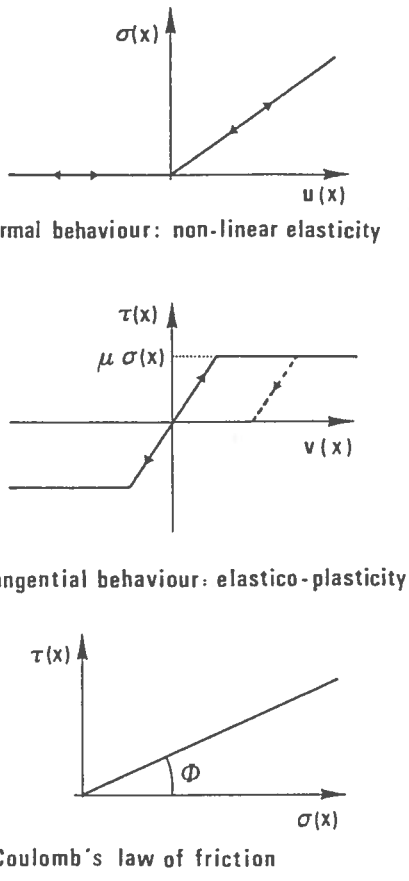

Fig. 2. Mechanical behavior law of a joint. Relationship between stresses and relative displacements at a point of abscissa x along the joint. Here $\sigma(x)$ is normal stress, $\tau(x)$ is shear stress, $u(x)$ is the normal component of the relative displacement, $v(x)$ is the tangential component of the relative displacement, ϕ is Coulomb's friction angle, and μ is Coulomb's coefficient of friction ($\mu = \tan\phi$).

to calculate displacements are introduced in the first part of this paper. In the second part the model is applied to the well-documented eruption of Mount St. Helens volcano (March–May 1980). Four models were created to study the effect of systematic variations in the values of some of the parameters on the computed displacement field. The results are discussed and compared with the measured pattern of deformation of the volcano. In the third part, some results from these models are used to formulate general remarks concerning the relationship between the structure of the magma storage system and the surface displacement field of volcanoes.

Method of Modeling

The Bloc method simulates the mechanical behavior of heterogeneous and fissured media under thermal or mechanical loadings, such as gravity, pressures, or any other force [*Pouyet et al.*, 1983]. Such a medium is modeled by an assemblage of blocks. The main assumption built into the program is therefore that all displacements occur at block boundaries only. In a two-dimensional planar strain model, such as the one used here, each block has three degrees of freedom, two degrees of translation within the plane, $X(i)$ and $Z(i)$, and one degree of rotation around its center of gravity, $\theta(i)$. Using the above assumption, it is possible to describe the kinematics of the structure divided into N number of blocks by the vector $\mathbf{X}$, composed of $3N$ degrees of freedom of the edifice.

Consider that incremental external forces (weight, pressure, acceleration, etc.) are being applied to the structure from an initial state described by the vector $\mathbf{X}_0$. These forces are expressed in the form of concentrated efforts $\Delta F_x(i)$, $\Delta F_z(i)$ and moments $\Delta M(i)$ applied to the center of gravity of each block, to form the vector $\Delta\mathbf{F}^{ex}$ of incremental external forces. The problem to be solved now is to compute the vector of the final deformed state by adding the resulting incremental displacements $\Delta\mathbf{X}$ to the initial state $\mathbf{X}_0$.

Considering the case of two blocks, numbered 1 and 2, in contact along joint j (Figure 1) and assuming that they undergo incremental displacements described by the vector $\Delta\mathbf{X}_{12}$:

$$\Delta\mathbf{X}_{12} = (\Delta X_1, \Delta Z_1, \Delta\theta_1, \Delta X_2, \Delta Z_2, \Delta\theta_2) \tag{1}$$

The basic assumption of rigid blocks gives the equation

$$\Delta\mathbf{U}_j = \mathbf{B}_j\Delta\mathbf{X}_{12} \tag{2}$$

where $\Delta\mathbf{U}_j$ is the vector of components (ΔU, ΔV, $\Delta\theta$) expressing the deformation of the joint at its midpoint 0 (ΔU and ΔV are relative displacements of the two faces in the normal and tangential directions, and $\Delta\theta$ is the relative rotation of the two faces; see Figure 1).

It is now possible to calculate the relative displacements of the two faces at the point of abscissa x along the joint, as follows:

$$\begin{aligned}\Delta u(x) &= \Delta U + x\Delta\theta \\ \Delta v(x) &= \Delta V\end{aligned} \tag{3}$$

Taking into account the mechanical behavior laws of the joint, it is possible to relate the normal stress $\Delta\sigma(x)$ and the shear stress $\Delta\tau(x)$ to the deformation of the joint. These laws are represented in Figure 2.

The normal behavior is nonlinear elastic.

For the closed part of the joint (i.e., if $\Delta u(x) \geq 0$),

$$\Delta\sigma(x) = k_n\Delta u(x) \tag{4}$$

where $k_n = E/e$ is normal stiffness, E is Young's modulus, and e is distance between the centers of gravity of the blocks.

For the open part of the joint (i.e., if $\Delta u(x) < 0$),

$$\Delta\sigma(x) = 0 \tag{5}$$

In contrast, the tangential behavior is elastoplastic, with Coulomb's friction.

Within the elastic limit (i.e, if $\Delta\tau(x) < \mu\Delta\sigma(x)$),

$$\Delta\tau(x) = k_t\Delta v(x) \tag{6}$$

where $k_t = G/e$ is shear stiffness, G is shear modulus, and μ is Coulomb's coefficient of friction.

Beyond the plastic limit (i.e, when slip occurs),

$$\Delta\tau(x) = \mu\Delta\sigma(x) \tag{7}$$

By integrating these stresses over x and taking (3)–(7) into account, a relation is obtained between $\Delta\mathbf{N}_j$ (vector composed of the normal force ΔN, the shear force ΔT, and the bending moment ΔM within the joint) and the deformation of the joint $\Delta\mathbf{U}_j$:

$$\Delta\mathbf{N}_j = \mathbf{D}_j\Delta\mathbf{U}_j \tag{8}$$

where $\mathbf{D}_j$ is the stiffness matrix of the joint.

Finally, the assumption of rigid blocks allows us to fully impart the efforts within the joint toward the centers of gravity of the two blocks, giving the vector of internal efforts $\Delta\mathbf{F}_{12}{}^{in}$:

$$\Delta\mathbf{F}_{12}{}^{in} = \mathbf{B}_j{}^t\Delta\mathbf{N}_j \tag{9}$$

where $\mathbf{B}_j{}^t$ is the transposition of $\mathbf{B}_j$ introduced in (2).

Taking (2) and (8) into account in (9) yields

$$\Delta\mathbf{F}_{12}{}^{in} = \mathbf{B}_j{}^t\mathbf{D}_j\mathbf{B}_j\Delta\mathbf{X}_{12} \tag{10}$$

Equation (10) expresses the relation between the displacements $\Delta\mathbf{X}_{12}$ of the two blocks and the resulting nodal internal forces $\Delta\mathbf{F}_{12}{}^{in}$ due to the deformation of the joint.

Writing (10) for every joint of the structure and joining all these equations give the overall mechanical behavior law for the assemblage of blocks:

$$\Delta\mathbf{F}^{in} = \mathbf{D}\Delta\mathbf{X} \tag{11}$$

where $\mathbf{D}$ is the overall stiffness matrix.

In order to obtain mechanical equilibrium, external forces and internal forces have to be equalized:

$$\Delta\mathbf{F}^{ex} = \Delta\mathbf{F}^{in} \tag{12}$$

or, according to (11),

$$\Delta\mathbf{F}^{ex} = \mathbf{D}\Delta\mathbf{X}$$

where $\Delta\mathbf{F}^{ex}$ is the vector of the applied external incremental forces, $\Delta\mathbf{X}$ the vector of the resulting incremental displacements of the blocks, and $\mathbf{D}$ the stiffness matrix of the structure. The physical meaning of this equation is that the structure reaches a state of equilibrium when the internal forces $\mathbf{D}\Delta\mathbf{X}$ induced within the edifice by the displacements $\Delta\mathbf{X}$ exactly balance the applied external forces $\Delta\mathbf{F}^{ex}$.

The problem is, however, nonlinear because the stiffness matrix $\mathbf{D}$ is a function of the solution $\Delta\mathbf{X}$. This nonlinearity has two consequences: (1) an iterative method has to be used to solve the problem, thus making for lengthy computations, and (2) the final outcome may depend on the loading path taken. As a consequence, it is necessary to increase the loads gradually up to full loading to follow as closely as possible the natural loading path.

Finally, it must be emphasized that the model only allows for displacements and rotations of small magnitudes. This restriction is not of great importance when the method is applied to volcanoes because the displacements are generally several orders of magnitude less than the size of the edifice itself.

APPLICATION TO MOUNT ST. HELENS

Mount St. Helens' 1980 eruption was found to be the best example to test the ability of this model to predict surface displacements measured during a volcanic crisis, since it is the best documented eruption in history.

Summary of Events

Pre-eruptive period (March 20 to May 17, 1980). The volcano became active in late March 1980, with seismic activity that rapidly increased to a high level [*Christiansen and Peterson*, 1981]. Most of the events were at shallow depths (less than 2.5 km deep), and the epicenters were concentrated on the north flank of the volcano [*Crosson et al.*, 1980; *Endo et al.*, 1981]. During the following 2 months, these earthquakes were accompanied by intermittent phreatic eruption from a summit crater and by intense deformations of the summit area and north slope. Photogrammetric surveys by *Moore and Albee* [1981] showed that a fracture system defining a graben was bisecting the summit area and that the upper north flank was bulging outward (Figure 3*a*). On April 25, *Lipman et al.* [1981] started ground displacement surveys. These revealed clear evidence of large-scale subhorizontal displacements in the bulge area at rates of 1.5–2.5 m/d, whereas the other parts of the volcano remained unchanged.

The concentration of hypocenters, the localized bulge of the upper north slope, and the subhorizontal nature of the displacements were interpreted early on as reflecting a forcible intrusion of magma within the volcano edifice. Because of the resulting excessive steepening of the north slope, the possibility of a gravitational failure and landslides in the inflated area was recognized at an early date [*Decker*, 1981; *Miller et al.*, 1981].

May 18 eruption. Without any warning and without any particular change in the deformation rates, an earthquake of magnitude 5.2 triggered the rapid series of events illustrated in Figure 3. The north slope of the volcano was affected by successive slope failures [*Voight et al.*, 1981] and giant landslides (Figure 3*b*). The pressure release associated with these slide movements resulted in hydrothermal and magmatic explosions, which produced a blast directed northward (Figure 3*c*). Consequently, the topography of the volcano was completely modified, since the eruption had created a large amphitheater-shaped crater within the north flank (Figure 3*d*).

Most of the data required for modeling purposes were available for this particular eruption. In particular, the geological structure was sufficiently well known to divide the edifice into blocks, and the existence of ground deformation data made it possible to compare the measured and computed displacements. The ability of the model to simulate deformations of a volcanic edifice could therefore be tested.

An initial model was developed, making certain assumptions regarding the values of some unknown parameters. During a second phase, three other models were constructed in order to study the parameter dependence of the results.

Best Fitting Model

Description of model 1. Because of the asymmetric behavior of Mount St. Helens during the eruption, a two-dimensional planar strain analysis was chosen. The geometry of the model was derived from a north-south geological cross section of the volcano in its initial state before the start of the

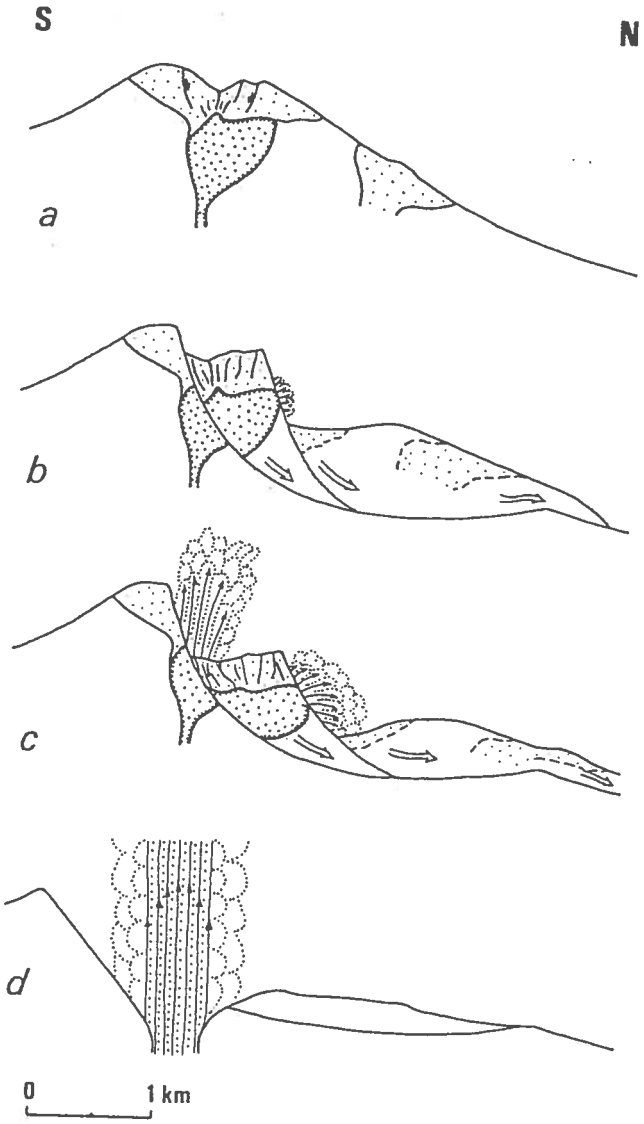

Fig. 3. Changes in the north-south profile of Mount St. Helens during the morning of May 18, 1980. (*a*) Before the eruption, showing the intrusion of a lava dome, the resulting apical graben, and north flank bulge. (*b*) About 20 s after landsliding began. (*c*) About 30 s after landsliding began, showing massive explosions. (*d*) After landsliding has exposed the main volcanic conduit (according to *Moore and Albee* [1981]).

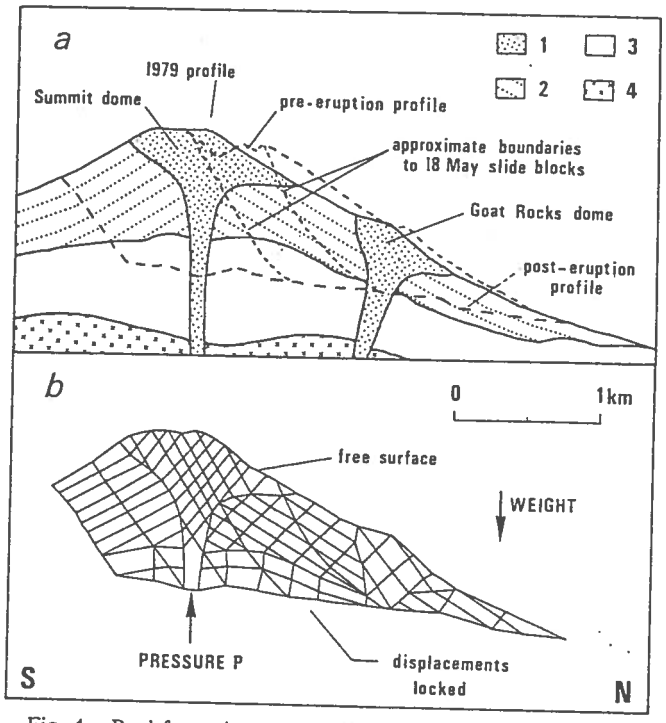

Fig. 4. Predeformation geometries. (*a*) Cross section of the volcano showing August 1979 profile, May 18 pre-eruption and posteruption profiles, geological discontinuities, and slide block boundaries: 1, dacite domes; 2, modern cone consisting of andesite and basalt lava flows, breccia, and scoria; 3, older Mount St. Helens volcanic center consisting of a complex of dacite dome remnants with glowing avalanche deposits, debris flows, and cross-cutting dykes; and 4, Tertiary bedrock (according to *Voight et al.* [1981]). (*b*) Initial geometry of model 1 derived from the above geological cross section and boundary conditions. The structure has already been subjected to its deadweight. The increase in magmatic pressure is about to begin in the central conduit.

crisis. The geological setting is shown in detail in Figure 4*a*. According to *Mullineaux and Crandell* [1981], the volcano consisted of two parts. An older complex of ancestral dacitic domes referred to as "older Mount St. Helens" underlay a younger part (the "modern cone"), consisting of dacitic domes (Summit dome and Goat Rocks dome) and alternating flows of andesite and basalt. The model shown in Figure 4*b* is derived from this cross section. Because the southern flank of the volcano had remained unaffected by deformation, the model is restricted to the part removed by the eruption. The resulting topography after the May 18 event is chosen to be the lower limit of the model, despite the fact that no discontinuity in the volcano prior to May 18, 1980, is known to correspond to this level. The effects of modifying this boundary are tested in model 3. The main geological discontinuities used to define certain block boundaries are the interface between the older and the modern cones, the limits of Summit and Goat Rocks dacite domes, and certain schematic bedding limits, assumed to result from alternating lava flows. Certain other block boundaries represent potential discontinuities that appeared because of the eruption. This is the case with the fracture system of the Summit dome, its surface geometry has been described by *Voight et al.* [1983], and it is assumed that this extended downward with the same dip. The potential discontinuities also include approximate boundaries of slide blocks of the May 18 gravitational landslides, as inferred by *Voight et al.* [1981] from photographs taken by eyewitnesses. Hypothetical discontinuities are added finally for reasons of symmetry. Goat Rocks and older Mount St. Helens are divided into blocks with fractures nearly perpendicular to the stratification planes. The resulting model (model 1) thus comprises 153 blocks with 459 degrees of freedom. The consequences of some variations in this geometry are examined with a simplified model (model 2).

The boundary conditions are (see Figure 4*b*) free surface on the upper bound (pre-May 18 topography) and displacements locked beyond the lower bound. In practice, this latter condition is imposed by preventing all blocks beyond this limit from moving (these blocks do not appear in the figures but are in the model). This condition means in particular that the entire south flank is regarded as perfectly undeformable. The effects of such a condition are tested with model 3, where the deformability of the south flank is taken into account.

Although the computer program can deal with blocks that have different mechanical properties, it was assumed (in view of the lack of adequate information about the mechanical con-

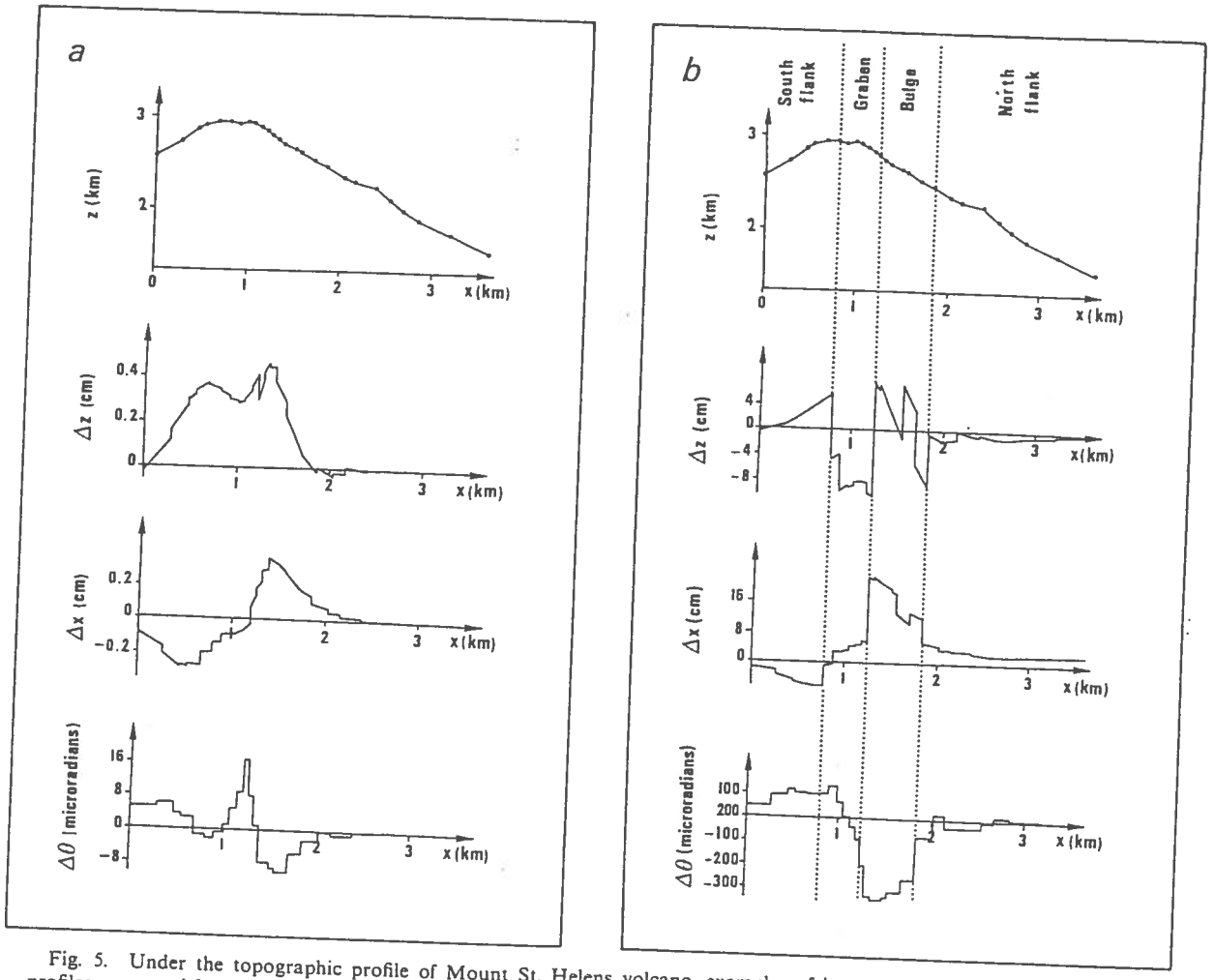

Fig. 5. Under the topographic profile of Mount St. Helens volcano, examples of incremental surface displacement profiles computed from model 1 during the rise in pressure. (*a*) Vertical component (Δz) and horizontal component (Δx) of the displacements and rotations ($\Delta\theta$) induced on the surface by increasing the pressure from 45 to 50 MPa. These profiles are typical of the first phase of deformation with relatively continuous profiles. (*b*) Surface displacements induced by increasing the pressure from 70 to 75 MPa. These profiles are typical of the second phase of deformation, with clear discontinuities along the profiles due to major displacement along the limits of the blocks.

stants of the different constituents of the volcano) that the whole edifice was made of a single material. Laboratory tests conducted by *Murase and McBirney* [1973] on rock samples collected from a volcano near Mount St. Helens provided the values of the mechanical constants of the joints: Young's modulus, $E = 30{,}000$ MPa, and Poisson's ratio, $\nu = 0.3$.

However, Coulomb's coefficient of friction on the joint planes remained unknown despite direct shear tests conducted in the laboratory on rock samples taken from the volcano by *Voight et al.* [1983]. Such tests give only the internal coefficient of friction, which differs from the coefficient of friction needed for discontinuities. In order to ascertain this coefficient, limit equilibrium stability analyses were carried out on the assumed slip surfaces of the May 18 landslides (Figure 4*a*) by the *Spencer* [1967] method. The lowest value required for the stability of the north slope under its deadweight is friction angle $\phi = 27°$ and coefficient of friction $\mu = \tan\phi = 0.5$. This minimum value is tested with model 1. The effect of a greater coefficient of friction ($\mu = 1$) is tested with the fourth model.

The structure was subjected to its deadweight in the first step of the mechanical loading procedure. This density was assumed to be uniform and equal to 2.2 g/cm^3, as inferred by *Voight et al.* [1981] from measurements on samples of the avalanche deposit, for the original cone material. The resulting deformed structure is plotted in Figure 4*b* and represents the initial state of deformation. All displacements referred to in this paper are relative to this initial state.

The rise of the lava dome into the central conduit of the volcano was simulated by application of a vertical pressure to the joint situated at the intersection of the central conduit and the lower bound of the model (Figure 4*b*). Pressure was also introduced into open joints to simulate the infiltration of magmatic gases. The pressure increased, in steps, from 1 to 5 MPa, and the displacement field was computed for each step. The computations stopped when the iterative method of resolution diverged, meaning that the pressure applied was too high for the structure to reach a state of equilibrium. Failure was then said to occur.

The May 18 earthquake was simulated by horizontal forces applied to each block in a northerly direction. These forces were computed from the product $n_s W$, where n_s is the seismic coefficient and W the weight of the block. Different deformed structures obtained at various steps during the rise in pressure were subjected to these ground accelerations. According to *Voight et al.* [1983], ground accelerations of more than 0.2 g were not unrealistic for the May 18 event. Calculations were thus carried out with n_s values ranging from 0.05 to 0.5. However, it must be borne in mind that this way of simulating

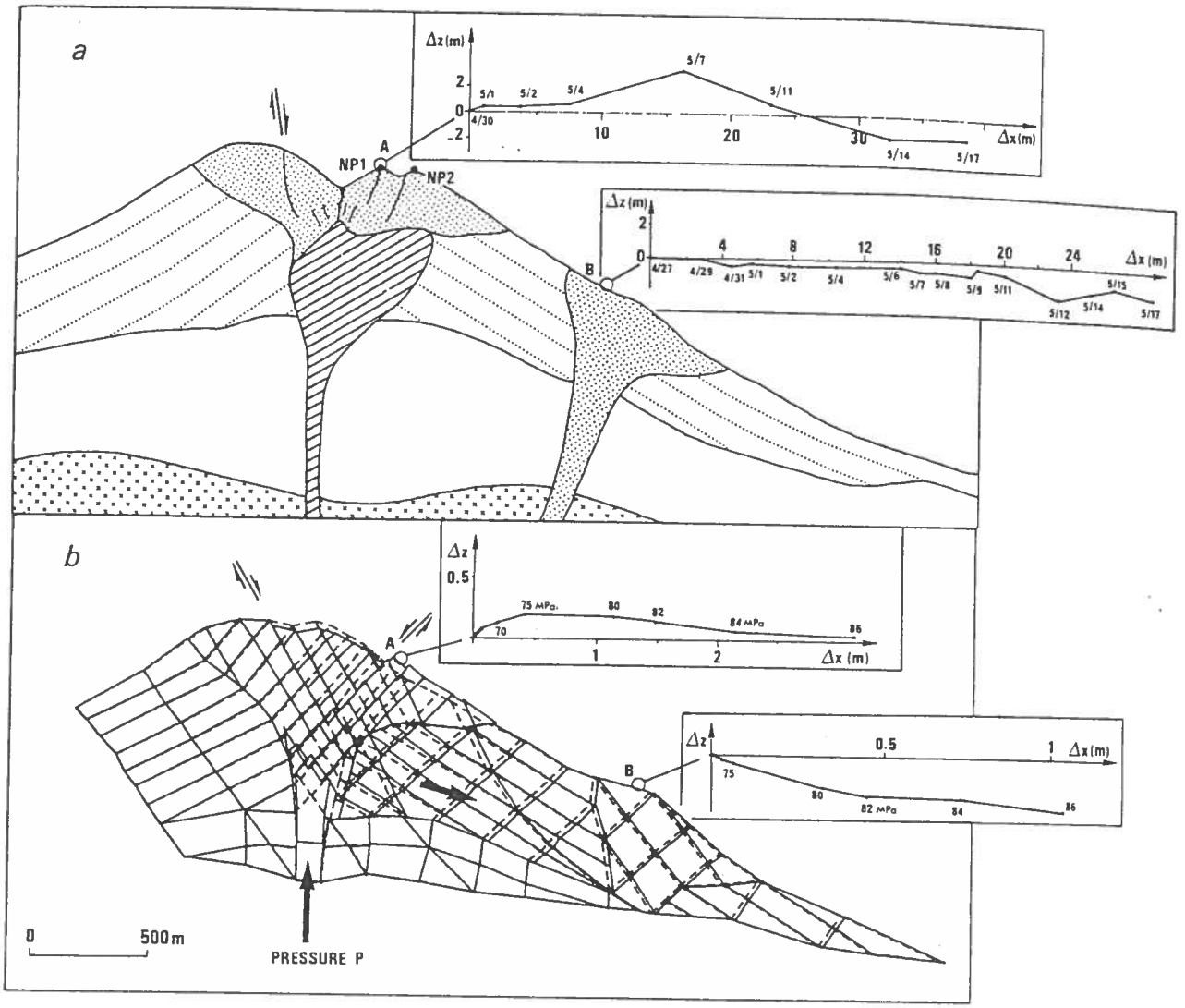

Fig. 6. Deformations observed during loading with magmatic pressure. (*a*) Schematic cross section of Mount St. Helens just before the May 18 eruption. The lava intrusion is indicated by shading. Plots of displacements in the N-S cross section measured at North Point (point A) and Goat Rocks (point B) geodetic targets from April 27 (4/27) to May 17 (5/17) are inserted (modified from *Moore and Albee* [1981] and *Lipman et al.* [1981]. (*b*) Deformed grid of model 1 under the internal pressure $P = 86$ MPa (solid line) superimposed on the initial state (dashed line). Displacements are multiplied by 20. Plots of computed displacements of points A and B induced by the rising pressure are inserted for comparison.

transitory earthquake loading by static forces remains crude; both the direction and magnitude of the ground acceleration probably varied in time and space within the volcano during the earthquake. In fact, this assumption is commonly made for limit equilibrium analysis in civil engineering studies.

Results. Two phases can easily be distinguished when observing the model progressively deforming under magmatic pressure.

For moderate values of the applied pressure (0–60 MPa), the surface of the edifice undergoes a general but slight swelling. Two inflation centers located on both sides of the summit are clearly visible in Figure 5*a*, where incremental surface displacements are plotted against horizontal distance along the profile of the model. The Δz indicates the vertical component of displacement resulting from a pressure increment, whereas Δx indicates the horizontal component, and $\Delta\theta$ the incremental ground tilt northward ($\Delta\theta < 0$) or southward ($\Delta\theta > 0$). The total magnitude of vertical displacement reached at 60 MPa does not exceed 5 cm. Such a homogeneous and slight swelling probably results from the interlocking of rock blocks within the Summit dome.

The second phase (65–90 MPa) could be called the plastic phase because numerous joints are just starting to exceed their elastic limit. This is obvious on the corresponding surface displacement profiles plotted in Figure 5*b*, where numerous discontinuities now appear between neighboring points. These discontinuities divide the surface into four zones, exhibiting different displacement features from south to north.

1. The south flank swells gently, the total amount of displacement due to the total rise in pressure remaining less than 10 cm.

2. The summit zone collapses by sliding along the northerly dipping joints of the Summit dome (Figure 6*b*). For this reason it will be referred to as the graben zone. The collapse is considerable: the cumulative vertical displacement with pressure rising from 0 to 84 MPa reaches 130 cm. The graben propagates to the north during the rise in pressure, and consequently, two high points appear in the topography of the upper north flank (Figure 6*b*). This feature concurs with the deformation observed on Mount St. Helens. According to *Christiansen and Peterson* [1981], a high point that had formed in late March just north of the summit (NP_1, shown as

point A in Figure 6*a*) subsided during April, while a second one (NP_2 in Figure 6*a*) began to form further north.

3. The upper part of the north slope bulges outward considerably. Its movement is the result of nearly horizontal northerly displacements, as shown in Figure 6*b*. The magnitudes of the horizontal displacements calculated in the bulge zone are quite high (up to 240 cm when the pressure rises to 84 MPa, for example). Major ground tilts of as much as 2700 μrad (cumulative rotations when pressure increases from 65 to 84 MPa) accompany these displacements (Figure 5*b*). Discontinuities visible on the vertical displacement profile in this bulge zone occur because the northernmost block of the Summit dome (see Figure 4*b*) is not sufficiently imbricated within the structure.

4. The lower part of the north flank slowly slides on the bedding limits when pressure increases up to 75 MPa. The amplitudes of these displacements then increase rapidly during the final part of the pressure rise, when two blocks forming a "corner" in the chimney make the whole north flank slip along the interface between the older Mount St. Helens and the modern cone (Figure 6*b*).

The pattern of failure under magmatic pressure alone (for $P = 90$ MPa) is then obvious: a large landslide affects the whole north slope of the volcano. It should be noted that this excess pressure value cannot be considered a reliable result of the model simulation, since it depends upon too many parameters (area of the joint where it is applied, depth of this joint, orientation of the joints within the Summit dome, etc.).

The same landslide on the north slope occurs when a low seismic acceleration (0.1 g) is applied to the model already deformed by a magmatic pressure of 75 MPa.

Discussion. This section deals with the comparison between displacements observed on Mount St. Helens and displacements calculated from this first model. The early phase of general swelling revealed by the model was not detected on the volcano, but ground displacement measurements may have started a little late (April 25) to show such an early uplift. For the second phase, the observed and calculated surface deformations are quite similar. The north-south deformed cross section of the volcano on May 17 and the deformed model are plotted in Figure 6 for comparison. The modeling method is able to predict the collapse of an apical graben (and its late extension to the north) and the large mass translation of the north flank by subhorizontal displacements, all these deformations being observed on Mount St. Helens. To refine this comparison, the displacements of two points of the model (points A and B in Figure 6) were computed and compared with the displacements of the two corresponding natural points where geodetic measurements had been conducted in May 1980. These displacements are plotted in Figure 6 (insert). The shapes of the measured and computed curves show an overall similarity. However, the observed displacements are at least 1 order of magnitude greater than those predicted from the model. An explanation for such a discrepancy might be found in the modeling method, which cannot deal with displacements of magnitudes greater than the size of the blocks.

The failure mode of the volcano is now discussed. The model shows that in both cases, i.e., (1) with only an increase in magmatic pressure and (2) with an increase in pressure followed by a seismic acceleration, a landslide occurs on the north slope. Accurate study of the surface displacements before failure is needed in order to discriminate between these

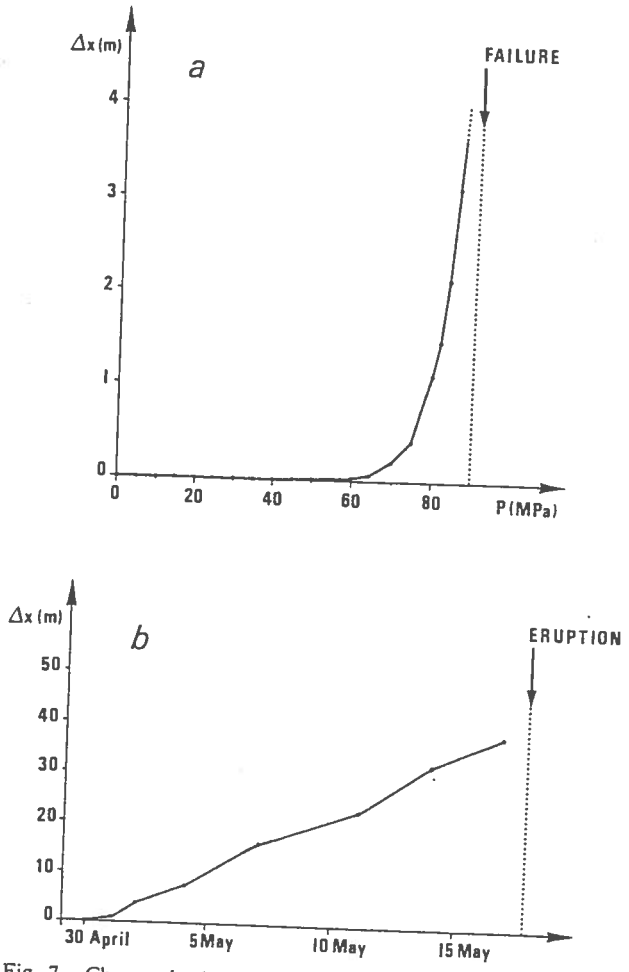

Fig. 7. Changes in the horizontal component of the displacement of North Point target (point A in Figure 6). (*a*) Plot of displacement computed with model 1 versus magnitude of the applied magmatic pressure. (*b*) Plot of the measured displacement versus elapsed time (modified from *Lipman et al.* [1981]).

two causes of failure. The horizontal component of the displacement computed at point A (see Figure 6 for location) is plotted versus the applied pressure in Figure 7*a*. If pressure increases in linear fashion with time, this curve is analogous to the plot of displacement versus time. It can be noted that the displacement accelerates considerably in this case when the movements of the north slope are triggered by the magmatic pressure. In contrast, observations showed that the displacement rate had remained quite constant until the day the eruption occurred (Figure 7*b*). This lack of acceleration indicates that an external factor was needed to induce instability and failure of the north slope. This modeling confirms the results obtained by *Voight et al.* [1983]: the May 18 earthquake was probably this trigger.

Parameter Dependence of the Model

Geometry. Model 2 (Figure 8) was developed in order to study the influence of the geometry of the discontinuities on the predicted pattern of deformation. This geometry was simplified. The model was restricted to the modern cone, and its lower bound then corresponded to the interface between the modern and older cones. Goat Rocks dome was eliminated from the north flank since it did not seem to play an important part either in the natural deformation [*Jordan and Kieffer*, 1981] or in model 1. The bounding surfaces for slide de-

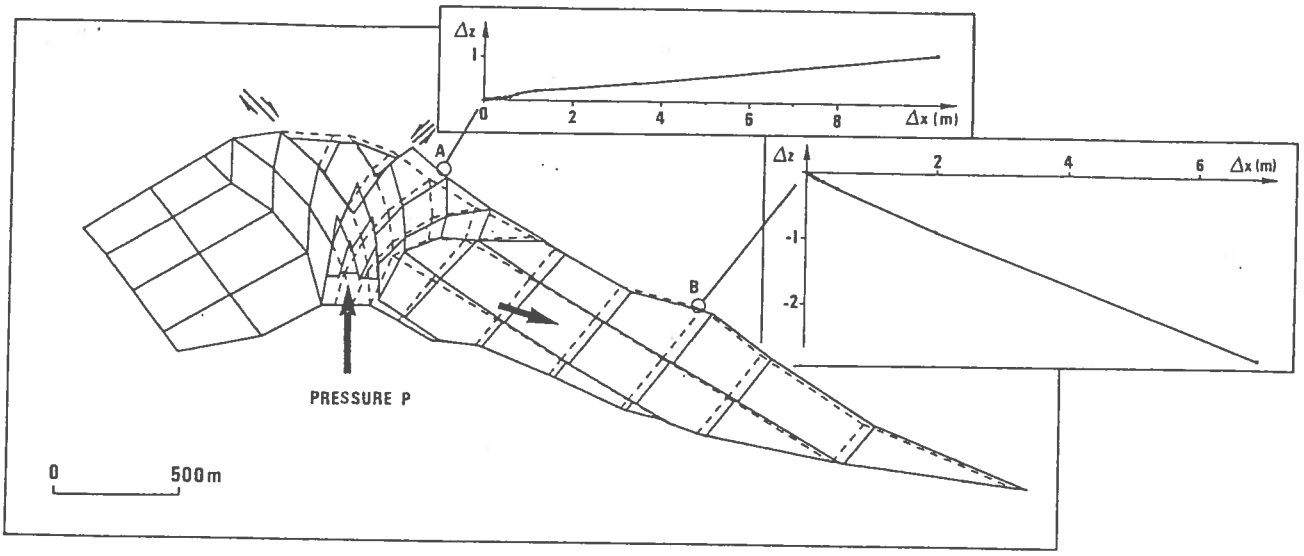

Fig. 8. Effect of simplified geometry. Deformed grid of model 2 computed for pressure $P = 27$ MPa within the central conduit and $P = 9$ MPa within the two open joints north of the conduit. The initial state (edifice loaded only with its deadweight) is superimposed in the form of the dashed line. Displacements are multiplied by 20. The displacements of North Point (point A) and Goat Rocks (point B) targets computed during the rise in pressure are shown.

tachments of May 18, whose location and even existence were too hypothetical, were also removed. Finally, the geometry of the fracture network affecting the Summit dome was modified. The lava dome intruding into the summit dacitic dome was compared with a rigid die indenting a homogeneous body, the theoretical geometry of the slip lines induced by this indentation being used to construct a new fracture network for the Summit dome. The resulting simplified geometry plotted in Figure 8 comprises only 49 blocks, i.e., 147 degrees of freedom. The other parameters (boundary conditions and mechanical constants) keep the same values as in model 1.

This structure was then loaded with its deadweight and with the step-by-step pressure increase simulating forcible intrusion of magma.

The results of these simulations show an overall similarity to the pattern of deformation in model 1. Two phases may again be distinguished, separated by the initiation of the graben collapse. The early uplift of the summit zone is much shorter than in model 1 (0–5 MPa), and the magnitude of inflation does not exceed a few millimeters. This difference probably originates in the geometry of the fracture network of the Summit dome. Since the slips along joints within the dome are easier in model 2, the blocks are less inclined to interlock (and the surface to swell) than in the first model. On the other hand, displacement profiles computed for the second phase (6–27 MPa) and plotted in Figure 9 are similar to profiles computed from model 1 (Figure 5*b*). Four zones with similar characteristics can again be distinguished: the south flank is slightly uplifted, an apical graben collapses to the north (cumulative downdrop for $P = 26$ MPa: 475 cm), and the upper part of the north slope bulges with northerly subhorizontal displacements, while small slides occur on the lower part.

Failure occurs again with the slope detachment of the whole north flank on the lower bound of the model. This instability is induced by the magmatic pressure alone as well as by the combination of pressure and seismic acceleration.

If a detailed comparison is made between the results of the two models, it appears that the refined grid spacing of model 1 yields a better fit to the real pattern of deformation. It can be related, for instance, to the appearance of two high points in

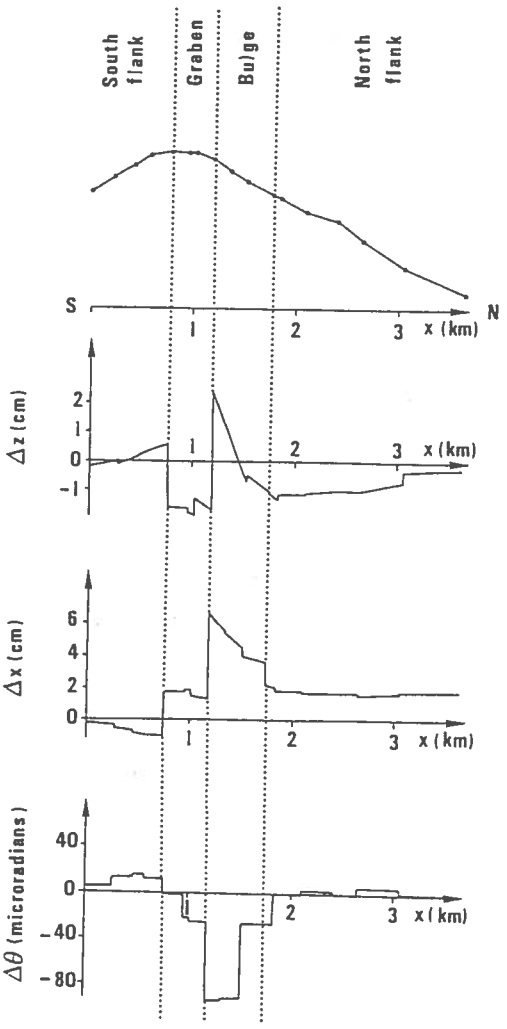

Fig. 9. Examples of incremental surface displacement profiles computed from model 2. These displacements are induced by the pressure increment from 23 to 24 MPa within the central conduit of the volcano. These profiles are typical of the plastic phase of deformation.

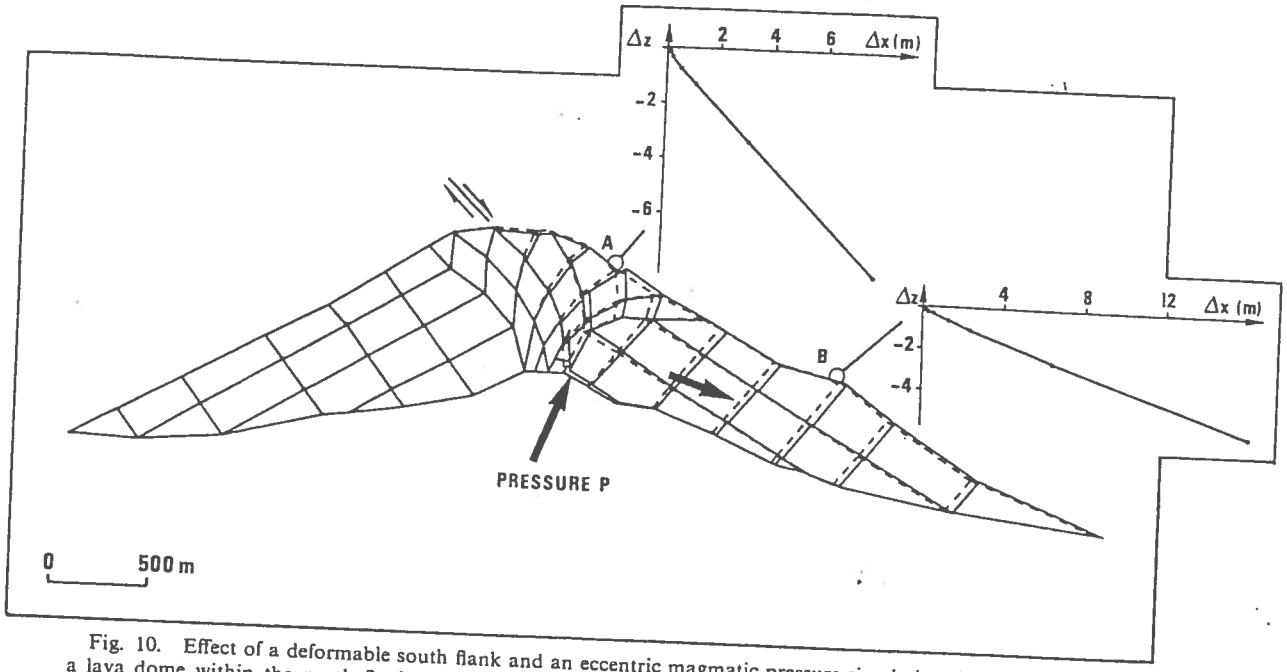

Fig. 10. Effect of a deformable south flank and an eccentric magmatic pressure simulating the asymmetric injection of a lava dome within the north flank. Deformed grid computed from model 3, for the magmatic pressure $P = 26$ MPa within the three open joints. Displacements are multiplied by 2. Computed displacements of North Point and Goat Rocks targets are shown.

the topography of the upper north flank associated with the late northward extension of the summit graben. These features appear in the results of model 1 (Figure 6*b*) but not in model 2 (Figure 8). In the same way, it is obvious from Figures 6 and 7 that model 1 gives a better fit between the computed and observed displacements of points A and B. This shows quite satisfactorily that, in general, the main features of the computed deformation pattern remain similar to those actually observed, even when simple geometry is used.

Boundary conditions in the south flank. According to most authors, the observed dissymmetry between the deformations of the north and south flanks resulted from the asymmetric position of the lava dome within the north flank. In order to test this statement, a third model was developed from the second (Figure 10). The new model extends southward to the point of intersection between the topography and the lower bound of the modern cone. So as to simulate the hypothesized northerly offset lava injection, the surface of application of the magmatic pressure was displaced slightly northward (Figure 10).

The incremental rise in pressure gives more or less the deformation mode expected. It again begins with a gentle and homogeneous swelling of the summit zone (from 0 to 17 MPa). A phase of plastic deformation then follows (18–27 MPa), where the surface may be divided into four zones, which are conspicuous on the displacement profiles plotted in Figure 11. The south flank remains nearly motionless (cumulative displacements less than 1 cm). An apical graben collapses with a cumulative downdrop amounting to 8 m just before failure occurs. It is wider than in the previous models and, consequently, includes point A, whose computed trajectory now differs considerably from the one measured (Figures 6 and 10). The upper north flank bulges as a result of subhorizontal displacements and pronounced ground tilts (Figure 11). The cumulative amplitude of this horizontal displacement reaches 22 m for $P = 26$ MPa. Small slides occur on the lower part of the north flank, as in the previous models.

Failure finally occurs in the usual way when the north slope slides on the lower bound of the model.

These results demonstrate that an asymmetric injection of lava, within the north flank, could explain the observed

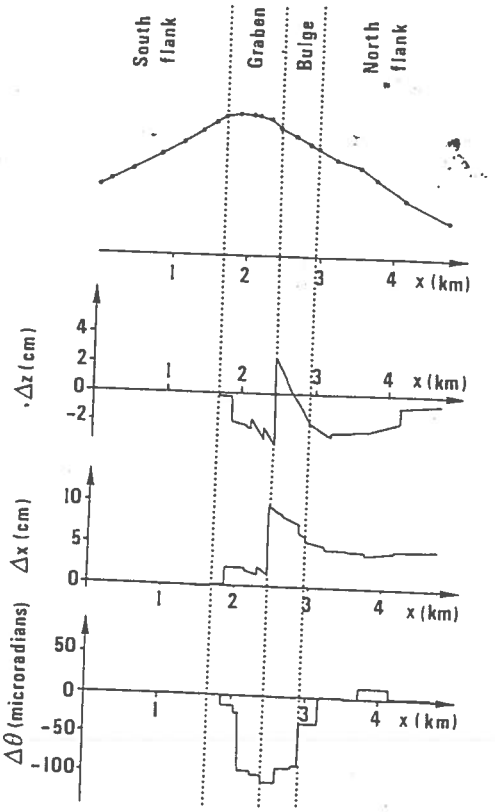

Fig. 11. Examples of incremental surface displacement profiles computed from model 3. These displacements result from the pressure increment from 22 to 23 MPa. The profiles are typical of the second phase of deformation.

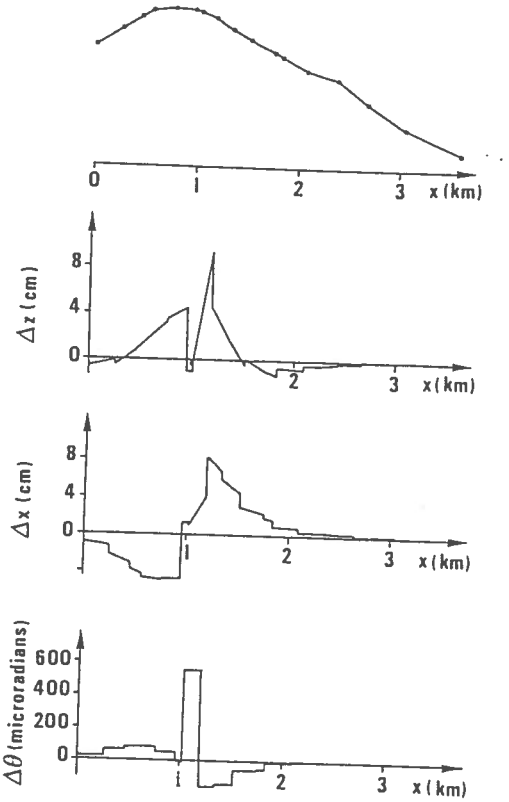

Fig. 12. Examples of incremental surface displacement profiles computed from model 4 when pressure rises from 20 to 25 MPa within the central conduit.

dissymmetric pattern of deformation. Moreover, this hypothesis is borne out by the existence of several domes in the northern half of the volcano, built asymmetrically over the last few thousand years [*Mullineaux and Crandell*, 1981]. Another possible cause of this dissymmetry could be the locking of the south flank combined with an axial injection of lava, both of which were boundary conditions introduced into models 1 and 2, but the origin of this locking phenomenon is not clear on Mount St. Helens. However, the results from these two models may be extended to volcanoes built on the slopes of pre-existing edifices, this particular location resulting in the locking of one of their flanks. The observations actually agree with our models, since gravitational instabilities of the unbuttressed flanks of Kilauea volcano and Piton de la Fournaise volcano (Réunion island, Indian Ocean) have been demonstrated by *Swanson et al.* [1976], *Vincent and Kieffer* [1978], *Chevallier and Bachelery* [1981], and *Duffield et al.* [1982].

Coefficient of friction. For lack of adequate data, the value $\mu = 0.5$ was used in models 1–3, since computations had shown that it was the lowest value required for the stability of the north slope under its deadweight. The influence of a higher coefficient of friction ($\mu = 1$) was tested with model 4, the other parameters keeping the same values as in model 2.

When magmatic intrusion is simulated, this new model behaves quite differently from the previous ones. Incremental surface displacement profiles keep the same general aspect from beginning to end of the rise in pressure (examples plotted in Figure 12). This means that the deformation scheme includes a unique phase that can be compared with the early phase of swelling in the previous models. The high friction makes slips along joints difficult, and this prevents the summit blocks from collapsing and the north flank from landsliding. Under the pressure rise, the summit of the edifice swells, and the distortion causes open fractures to form on the surface (Figure 13). A major crack also opens progressively between the north and south sectors of the model (joints 52 and 53 in Figure 13). Because this fracture is contiguous with the surface of application of the magmatic pressure, the intrusion of volcanic fluids is simulated by submitting its two faces to pressure. The crack then rapidly propagates up to the surface, and failure occurs when the central part of the model is quickly uplifted along this fracture and "blows up." When a seismic acceleration is associated with the rise in pressure, landslides only occur with the lowest values of the initial magmatic pressure. The vertical "explosion" of the Summit dome is inevitable with higher pressures, even when a horizontal seismic acceleration is applied.

The coefficient of friction obviously plays the most important role in the deformation pattern of the volcanic edifice. When this parameter is assumed to be equal to 1, neither the surface displacement process nor the failure pattern fits those observed on the volcano. These results suggest that within the limitations of the model (which does not take into account the pore fluid pressure, for instance) the coefficient of friction on

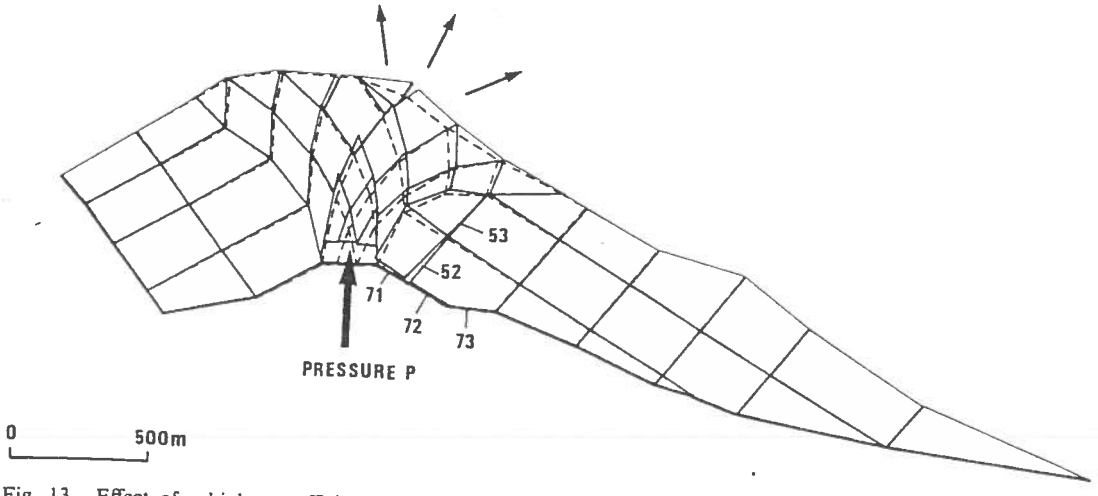

Fig. 13. Effect of a higher coefficient of friction ($\mu = 1$) on the pattern of deformation. Deformed grid of model 4 computed for the following value of magmatic pressure: $P = 35$ MPa within the central conduit and joint 71, 15 MPa within joints 52 and 72, and 5 MPa within joints 53 and 73. Displacement multiplied by 50.

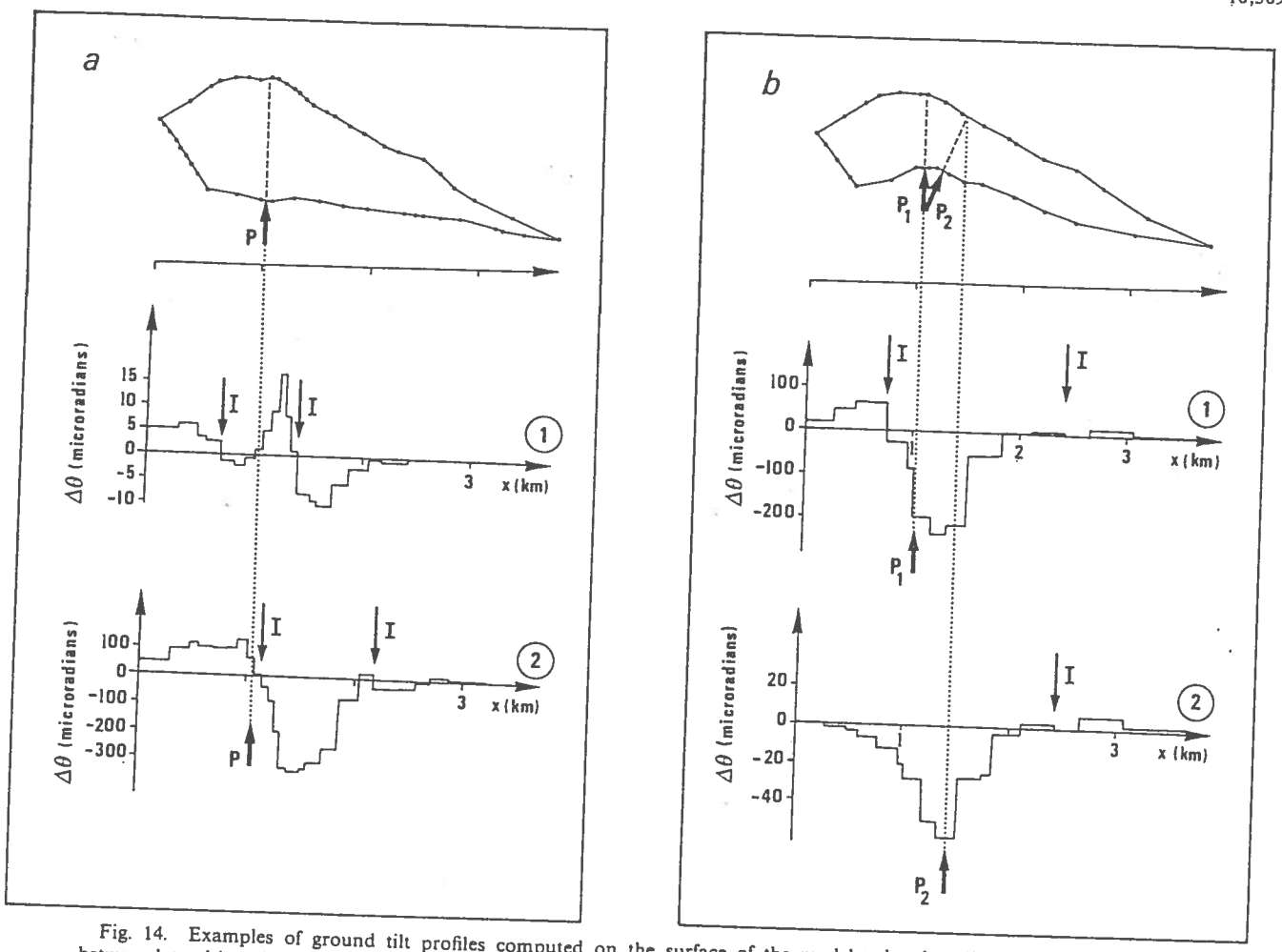

Fig. 14. Examples of ground tilt profiles computed on the surface of the models, showing different relationships between lateral locations of pressure source at depth and inflation centers on the surface. A short arrow (P) indicates the point where the line of application of the pressure force intersects the topographic profile. A long arrow (I) indicates an inflation center deduced from the tilt profile. (*a*) Tilt profiles computed from model 1 induced by the rise in pressure from 45 to 50 MPa (profile 1) and from 70 to 75 MPa (profile 2). (*b*) Tilt profiles are computed from model 2 for the following pressure increments: P_1 increases from 20 to 21 MPa within the central conduit (profile 1), and P_2 increases from 0 to 21 MPa within an open joint north of the conduit (profile 2).

discontinuities was, in that particular case, probably closer to 0.5 than to 1.

Surface Deformations and Volcanic Structures

In order to interpret surface deformation data it is commonly assumed that the volcanic edifice behaves in a homogeneous, isotropic, and elastic manner. For example, level surveys are used to map inflation centers, and assuming that these centers lie exactly above inflating magma reservoirs, inferences are drawn directly from these maps regarding the internal plumbing of the volcano. *Fiske and Kinoshita* [1969] reported, for example, that the center of inflation as determined on Kilauea volcano prior to its 1967–1968 eruption changed position repeatedly. They interpreted these lateral migrations as reflecting movements of magma within a complex of intersecting small reservoirs.

If mechanical heterogeneities and discontinuities of volcanic edifices are now taken into account, our models give the opportunity for studying the relationships between the locations of sources and the centers of inflation in such complex media. Ground tilt profiles were used to locate the inflation centers at the points where the tilt curve changes sign from positive to negative (see Figure 14). The position of this inflation center was plotted in this way for each incremental rise in pressure. Its lateral migrations during the entire pressure rise show the following.

1. The center of inflation can move laterally, or else the number of centers may actually change, without any modification in the load path. An example is given in Figure 14*a* (from model 1). Two inflation points are detected in the summit zone of model 1 when pressure rises from 45 to 50 MPa (profile 1 in Figure 14*a*), and there is only one left later, when pressure rises from 70 to 75 MPa (profile 2). This is in spite of the fact that the pressure source at depth does not move between these two steps. In this particular case, such a modification arises because many changes occur in the mechanical behavior of the model between these two increments, with initiation of the graben collapse.

2. The point where pressure is applied at depth can move without producing any related movement of the center of inflation on the surface. An example is given in Figure 14*b* (from model 2). When pressure (P_1) rises in the chimney from 20 to 21 MPa, two inflation centers can be detected near the summit and on the north flank (profile 1 in Figure 14*b*), but when pressure is being applied slightly northward (P_2) (because it is being introduced in an opening crack), the inflation centers do not move northward (profile 2 in Figure 14*b*).

These examples show that no close connection can be es-

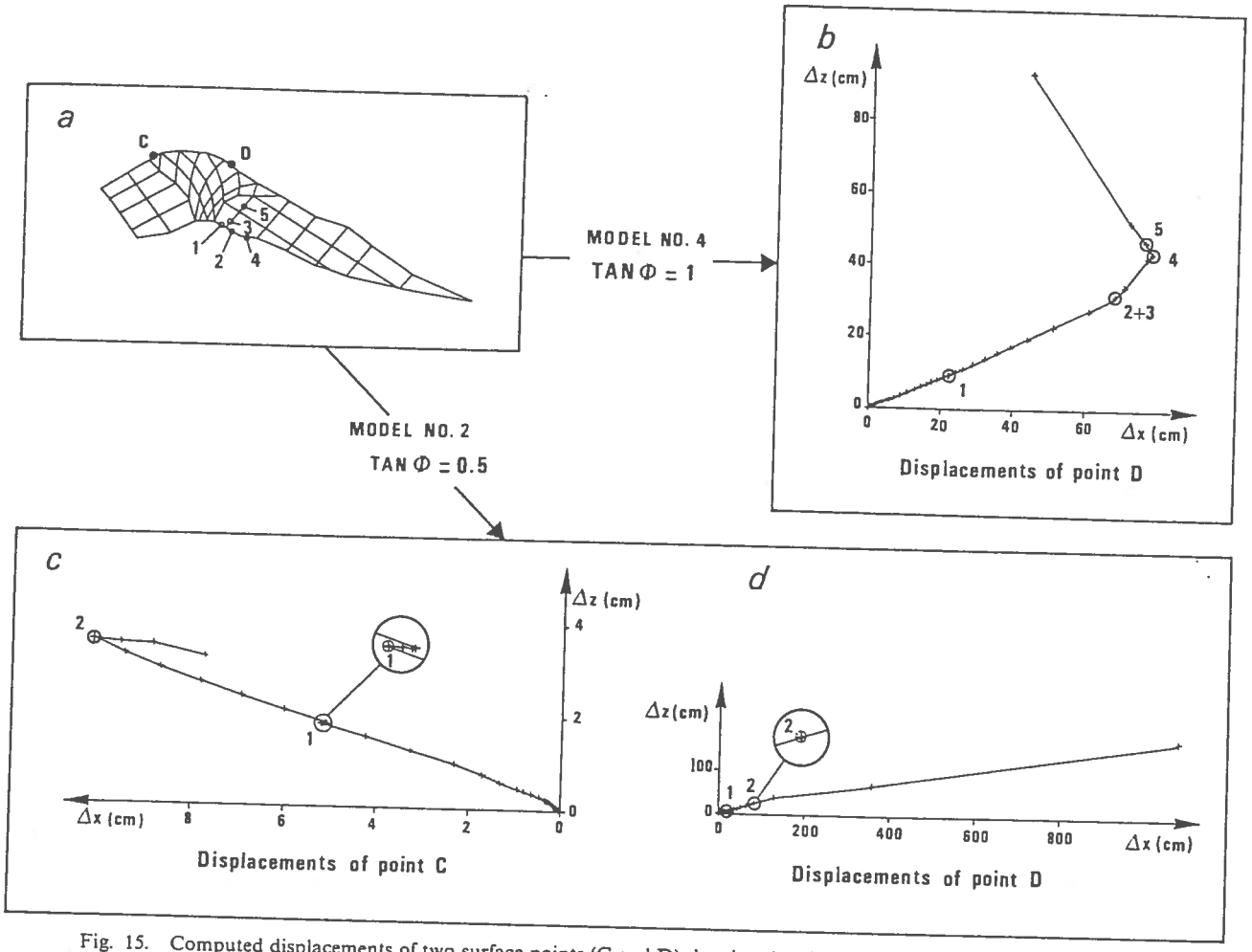

Fig. 15. Computed displacements of two surface points (C and D) showing the effect of introducing magmatic pressure within different open joints (numbered from 1 to 5). The displacements are induced by the incremental rise of pressure, and the points on each curve correspond to pressure increments. A circle around a point indicates that the introduction of pressure within an open joint begins and the number of this joint is given. (*a*) Geometry of models 2 and 4, showing the location of points C and D and the location of joints 1–5 where pressure was introduced. (*b*) Displacements of point D computed from model 4. Note the change in direction every time pressure is introduced into a new joint. (*c*) Displacements of point C computed from model 2. Note the sharp change in direction. (*d*) Displacements of point D computed from model 2. No modification occurs in the curve.

tablished between the location of the pressure source at depth and the position of the center of inflation on the surface, when the model takes mechanical discontinuities into account.

With regard to the possibility of studying surface displacements in order to obtain more information about the internal structure and functioning of a volcano, trajectories of surface points throughout the entire pressure rise may also be of interest. In this way, it is possible to look for changes in these displacements, reflecting modifications in the way pressure is applied at depth (when the introduction of magmatic fluids into opening cracks is simulated, for instance). Such studies have been carried out systematically with the results of our models, showing two typical types of behavior, as illustrated in Figure 15.

1. In model 4 (coefficient of friction $\mu = 1$), each computed trajectory shows clear changes every time pressure is introduced into a new open crack. The displacements of point D are plotted in Figure 15*b* and give clear evidence of such modifications.

2. In models 2 and 3 ($\mu = 0.5$), these modifications are not systematic. The movements of surface points belonging to highly deformed zones (summit and north flank) are insensitive to the introduction of magmatic pressure into cracks. This is the case for point D in Figure 15*d*. On the other hand, the trajectories of the points of the slightly deformed south flank show sharp changes of direction related to the introduction of pressure into cracks (point C in Figure 15*c*). These discrepancies result from the assumed elastoplastic behavior of the material. Below the elastic limit, the induced deformations vary in accordance with the applied loading. The surface displacements clearly reflect the propagation of magmatic fluids into cracks. Since model 4 has a high coefficient of friction and, consequently, high elastic limit, this linear mechanical behavior is retained. The south flanks of models 1–3 behave in a similar manner, as the stresses acting on them never exceed the yield stress of the material. In contrast, the summit and northern zones of these models rapidly reach the stage of plastic deformation where the stress-strain relationship is no longer linear. Their displacements cannot reflect the propagation of cracks.

In an effort to obtain information regarding the internal structure of volcanoes, recording displacements of the order of

a few millimeters in slightly deformed zones (Mount St. Helens' south flank, for instance) seems more important than interpreting major displacements in plastically deforming sectors. As a matter of fact, small displacements give a much better representation of the movements of magma within the volcanic edifice, but of course, the larger displacements are obviously of great interest for assessing eruption potential, since these displacements in theory accelerate considerably when failure approaches (Figure 7).

CONCLUSIONS

The Bloc method helps to improve the modeling of volcanic deformations, as it takes into account the discontinuities of the volcanic structures. However, the models remain simple in comparison with the complexity of natural edifices. For instance, they are only two-dimensional, despite the fact that the mechanical behavior of Mount St. Helens was clearly three-dimensional during the 1980 events. Moreover, the pore fluid pressure was not taken into account, although the volcano was probably saturated with water to a significant degree [*Moore and Sisson*, 1981]. Finally, the effect of increasing temperature close to the magmatic intrusion ($T > 900°$, according to *Eichelberger and Hayes* [1982]) could also have been considered. It is noteworthy that the Bloc method is able to deal with these complexities, but it was decided not to use such possibilities in order to avoid models with too many unknown parameters.

The calculated displacement fields obtained with the models (particularly model 1) are similar to the real ones measured before the eruption of May 18. Such results were obtained without any preconceived idea regarding the mechanical properties of the joints (since the same mechanical constants were used for all of them). Models with $\tan \phi = 0.5$ produced a deformation field that is consistent with the observations made on the volcano prior to eruption: the south flank was only slightly affected by magmatic intrusion, while the summit zone underwent a graben collapse and the upper north flank bulged outward considerably, with subhorizontal northerly displacements. The simulated and observed failure modes were also consistent, with a gravitational landslide of the entire north slope.

As a result of these similarities, the following conclusions may be drawn.

1. The basic hypothesis of the Bloc method of modeling proves to be correct in the case of the 1980 eruption of Mount St. Helens. Discontinuities definitely seem to play a more important role in the deformation mechanism than the mechanical properties of the continuous block material. Any other model assuming that the volcanic edifice is a continuum could predict the appearance of cracks by computing stresses within the structure but could not simulate slides along these fractures, such as the apical graben collapse occurring on Mount St. Helens. The Bloc method seems better adapted to simulating these discontinuous displacement fields, which often characterize volcanic surface deformations.

2. Some success was achieved by applying increasing pressure within the central conduit of the volcano. This shows that this type of loading, resulting from magmatic intrusion, was actually able to cause the precursory surface deformations observed on the volcano, as was assumed by researchers working there.

3. A good fit to the observed asymmetric displacement field is given by model 2 (undeformable south flank) as well as by model 3 (pressure applied asymmetrically within the north flank). Two explanations for the asymmetric deformations are thus possible. However, the second appears to be the more likely.

4. The coefficient of friction on the discontinuities on Mount St. Helens was probably nearer to 0.5 than 1, since when the latter value is chosen, neither the pattern of surface deformation (general uplift) nor the failure mode (summit explosion) fits the observations.

5. The modeling method shows that the use of internal pressure always ends with gravitational failure of the north slope. It may therefore be concluded that the injection of lava alone could have triggered this landslide, but in that case a precursory increase of the displacement rate would have given warning of the impending failure, and this was not the case on Mount St. Helens. These models show once again that the gravitational failure of the north slope was actually due to cumulative factors including magmatic pressure increasing to a stable state, and a trigger earthquake.

Nevertheless, it must be emphasized that the observed displacements largely exceed those predicted by the models. This discrepancy may be due to the actual modeling method, which cannot deal with large-magnitude displacements.

More generally, this modeling method yields some clues as to the relationship between the internal structure of a volcano and its surface displacement field. Such connections do exist, but they are not as clear when mechanical discontinuities are taken into account as when the volcano is assumed to be perfectly homogeneous and elastic. The only model to give a displacement field that clearly reflects the movements of magma (pressure) at depth is model 4, where the coefficient of friction is high ($\tan \phi = 1$). When this coefficient is low ($\tan \phi = 0.5$), only the slightly deformed zones remain sensitive to modifications in the loading. It is thus important to be able to detect displacements of very low magnitudes in order to have a better understanding of the manner in which the volcano functions. However, studies of major deformations must not be neglected either, since they give important indications for hazard assessments.

Finally, it must be borne in mind that these models of the eruption of Mount St. Helens proved to be successful thanks to the exceptional quantity and quality of data available. Such accurate simulation of the deformations of other volcanoes by this type of modeling method would be impossible because of the lack of adequate data concerning their initial structures. However, the development of simple and synthetic models can play a great part in furthering the understanding of some volcanic processes. They may be used, for example, to check that the hypotheses that researchers make about internal structures are compatible with surface deformations and the general laws of mechanics. They may also show which parameters play an important part in the deformation and failure modes and thus be a guide for further research.

Acknowledgments. We are greatly indebted to the management and engineers of Coyne et Bellier Consulting Engineers, who provided the Bloc program and computer. Reviews by P. T. Delaney, D. A. Swanson, and B. Chadwick helped in improving the manuscript. The work was supported by the Programme Interdisciplinaire pour la Prévision et la Surveillance des Eruptions Volcaniques of the Centre National de la Recherche Scientifique.

REFERENCES

Chevallier, L., and P. Bachelery, Evolution structurale du volcan actif du Piton de la Fournaise, Ile de la Réunion, Océan Indien Occidental, *Bull. Vulcanol.*, *44*, 723–741, 1981.

Christiansen, R. L., and D. W. Peterson, Chronology of the 1980 eruptive activity, *U.S. Geol. Surv. Prof. Pap., 1250*, 17–30, 1981.

Crosson, R. S., E. T. Endo, S. T. Malone, L. J. Noson, and C. S. Weaver, Eruptions of Mount St. Helens—Seismology, *Nature, 285*, 529–533, 1980.

Decker, R. W., The 1980 activity: A case study in volcanic eruption forecasting, *U.S. Geol. Surv. Prof. Pap., 1250*, 815–820, 1981.

Dieterich, J. H., and R. W. Decker, Finite element modeling of surface deformation associated with volcanism, *J. Geophys. Res., 80*, 4094–4102, 1975.

Duffield, W. A., L. Stieltjes, and J. Varet, Huge landslide blocks in the growth of Piton de la Fournaise, La Réunion, and Kilauea volcano, Hawaii, *J. Volcanol. Geotherm. Res., 12*, 139–142, 1982.

Dvorak, J., A. Okamura, and J. H. Dieterich, Analysis of surface deformation data, Kilauea volcano, Hawaii, October 1966 to September 1970, *J. Geophys. Res., 88*, 9295–9304, 1983.

Eichelberger, J. C., and D. B. Hayes, Magmatic model for the Mount St. Helens blast of May 18, 1980, *J. Geophys. Res., 87*, 7727–7738, 1982.

Endo, E. T., S. D. Malone, L. J. Noson, and C. S. Weaver, Locations, magnitudes and statistics of the March 20–May 18 earthquake sequence, *U.S. Geol. Surv. Prof. Pap., 1250*, 93–107, 1981.

Fiske, R. S., and W. T. Kinoshita, Inflation of Kilauea volcano prior to its 1967–1968 eruption, *Science, 165*, 341–349, 1969.

Jordan, R., and H. H. Kieffer, Topographic changes at Mount St. Helens—Large-scale photogrammetry and digital terrain models, *U.S. Geol. Surv. Prof. Pap., 1250*, 135–141, 1981.

Lipman, P. W., J. G. Moore, and D. A. Swanson, Bulging of the north flank before the May 18 eruption—Geodetic data, *U.S. Geol. Surv. Prof. Pap., 1250*, 143–155, 1981.

Miller, C. D., D. R. Mullineaux, and D. R. Crandell, Use of volcanic hazards assessment: A case study at an active volcano, *U.S. Geol. Surv. Prof. Pap., 1250*, 789–802, 1981.

Mogi, K., Relations between the eruptions of various volcanoes and the deformations of the ground surfaces around them, *Bull. Earthquake Res. Inst., Univ. Tokyo, 36*, 99–134, 1958.

Moore, J. G., and W. C. Albee, Topographic and structural changes, March–July 1980 photogrammetric data, *U.S. Geol. Surv. Prof. Pap., 1250*, 123–134, 1981.

Moore, J. G., and T. W. Sisson, Deposits and effects of the May 18 pyroclastic surge, *U.S. Geol. Surv. Prof. Pap., 1250*, H-21–H-38, 1981.

Mullineaux, D. R., and D. R. Crandell, The eruptive history of Mount St. Helens, *U.S. Geol. Surv. Prof. Pap., 1250*, 3–15, 1981.

Murase, T., and A. R. McBirney, Properties of some common igneous rocks and their melts at high temperatures, *Geol. Soc. Am. Bull., 84*, 3563–3592, 1973.

Murray, J. B., and A. D. Pullen, Three-dimensional model of the feeder conduit of the 1983 eruption of Mount Etna volcano from ground deformation measurements, *Bull. Volcanol.*, in press, 1987.

Pollard, D. D., P. T. Delaney, W. A. Duffield, E. T. Endo, and A. T. Okamura, Surface deformation in volcanic rift zones, *Tectonophysics, 94*, 541–584, 1983.

Pouyet, P., J. Picaut, J. L. Costaz, and J. Dulac, "Bloc" program for elasto-plastic calculations of fissured media, *Struct. Mech. React. Technol., 7th*, Chicago, 1983.

Ryan, M. P., J. Y. K. Blevins, A. T. Okamura, and R. Y. Koyanagi, Magma reservoir subsidence mechanics: Theoretical summary and application to Kilauea volcano, Hawaii, *J. Geophys. Res., 88*, 4147–4181, 1983.

Spencer, E., Method of analysis of the stability of embankments assuming parallel interslices forces, *Geotechnique, 17*, 1, 1967.

Swanson, D. A., W. A. Duffield, and R. S. Fiske, Displacement of the south flank of Kilauea volcano: The result of forceful intrusion of magma into the rift zones, *U.S. Geol. Surv. Prof. Pap., 963*, 39 pp., 1976.

Vincent, P. M., and G. Kieffer, Hypothése sur la structure et l'évolution du Piton de la Fournaise (Ile de la Réunion) aprés les éruptions de 1977, paper presented at the 6th Réunion Annuelle des Sciences de la Terre, Orsay, 1978.

Voight, B., H. Glicken, R. J. Janda, and P. M. Douglass, Catastrophic avalanche of May 18, *U.S. Geol. Surv. Prof. Pap., 1250*, 347–377, 1981.

Voight, B., H. Glicken, R. J. Janda, and P. M. Douglass, Nature and mechanics of the Mount St. Helens rockslide-avalanche of 18 May 1980, *Geotechnique, 33*, 243–273, 1983.

J. Boudon, Coyne et Bellier, 5 Rue d'Héliopolis, 75017 Paris, France.

J. P. Gratier and A. Paul, Institut de Recherches Interdisciplinaires de Géologie et de Mécanique, University of Grenoble, B.P. 68, 38402 St. Martin d'Héres Cedex, France.

(Received November 12, 1985;
revised June 2, 1986;
accepted June 9, 1986.)